Michael P. Manahan, Sr.[1]

Miniaturized Fracture Toughness Testing During the Plant Life Extension Period

REFERENCE: Manahan, M. P., **"Miniaturized Fracture Toughness Testing During the Plant Life Extension Period,"** *Small Specimen Test Techniques Applied to Nuclear Reactor Vessel Thermal Annealing and Plant Life Extension, ASTM STP 1204,* W. R. Corwin, F. M. Haggag, and W. L. Server, Eds., American Society for Testing and Materials, Philadelphia, 1993, pp. 199–213.

ABSTRACT: It is desirable to obtain plane strain fracture toughness data in support of plant refurbishment and plant life extension (PLEX) efforts. These data may be needed for pressurized thermal shock (PTS) analyses, low upper shelf energy analyses, and to verify shifts in the K_{IR} curve. A major impediment to the development of plant-specific fracture toughness data is the specimen size requirement and the fact that many surveillance capsule programs do not include fracture toughness specimens.

A new test has been developed to resolve these difficulties. An experimental modification, referred to as stress field modification, enables testing using specimens substantially thinner than those currently required by ASTM. Examination of the stress field modified specimen fracture surface demonstrates that plane strain conditions were achieved in the miniature specimens. The miniature specimens were machined from a nuclear-grade ASTM A508 steel used in the Oak Ridge National Laboratory pressurized thermal shock study. The miniature specimen data lie within the experimental scatter of the 6-in. (15.24 cm) vessel data. The development of this new fracture test enables plane strain testing of materials from surveillance programs (broken Charpy specimens) and from material cut from in-service components.

KEYWORDS: miniature specimens, fracture toughness, plane strain, stress field modification, *J*-Integral, finite element

In order to calculate pressure-temperature (P-T) operating limits, it is necessary to determine the temperature dependence of the lower bound to static and dynamic fracture toughness for the limiting beltline material. As stated in the ASME code, Section XI, Article A-4400, it is intended that plant-specific fracture toughness data be determined directly in the surveillance program. In particular, the ASME code states, "Radiation induced changes in fracture toughness should be determined from surveillance specimens of the actual material and product form, irradiated according to the surveillance techniques of ASTM E 185, Standard Recommended Practice for Effects of High-Energy Irradiation on the Mechanical Properties of Metallic Materials." Since most surveillance programs do not include fracture toughness specimens, the effects of neutron irradiation are considered for both K_{IA} and K_{IC} by shifting the reference nil ductility temperature (RT_{NDT}) as a function of irradiation using

[1] President, MPM Research & Consulting, 915 Pike Street, Lemont, PA 16851; Adjunct professor of nuclear engineering, The Pennsylvania State University, 231 Sackett Building, University Park, PA 16802.

[2] The techniques described in this paper are protected by U.S. Patent No. 4,885,027, entitled "Determining Plane-Strain Fracture Toughness and the J-Integral for Solid Materials Using Stress-Field-Modified Miniature Specimens."

trend curves. In particular, Regulatory Guide 1.99 (Revision 2) [RG 1.99(2)][3] is used to determine the Charpy shift at the 41-J level (ΔT_{41}) due to neutron damage. In cases where two or more credible surveillance data are available, the Regulatory Guide provides a procedure for combining the measured data with the generic model to predict the Charpy shift fluence dependence. As stated in ASME Section III, Article A-4400, this approach is intended to be extremely conservative: "These curves (the shifted K_{IA} and K_{IC} curves) are intended to be very conservative since the recommended procedure is to determine the irradiation effects from surveillance specimens of the actual material and product form in question." The curves referred to are the shifted ASME K_{IA} and K_{IC} reference curves. Further, as stated in article A-4200, these unirradiated curves are intended to be very conservative as well: "The curves in Fig. A-4200-I are intended to be very conservative since the recommended procedure is to determine the material fracture toughness from specimens of the actual material and product form in question." In addition, the shift in fracture toughness data due to irradiation of a pressure vessel steel, measured in accordance with ASTM Test Method for J_{IC}, a Measure of Fracture Toughness (E 813), does not compare well with the K_{IR} curve when shifted by the measured Charpy 40 J transition temperature shift [*1*]. In response to these concerns and to the need within the nuclear industry's plant life extension (PLEX) program for in-service materials data, a new approach to plane strain fracture toughness testing has been developed. The theoretical framework and initial benchmark data are presented in this paper. The approach described has been applied to determine static plane strain fracture toughness data using specimens substantially thinner than those required by ASTM. As shown in the ASME code, dynamic fracture toughness data are significantly more conservative than static data. However, analysis of the data and equations presented in Ref *2* reveals that static data can be used to represent crack arrest data for SA-533 Grade B Class 1, SA-508 Class 2, and SA-508 Class 3 steel by

1. Fitting the lower bound to the measured static fracture toughness data.
2. Decreasing the lower bound static fracture toughness data by ~10 MPa $\sqrt{m}$.
3. Translating the lower bound fit 24°C to the right.

Thus, data obtained using the static testing approach described herein can be mapped into dynamic data by using the procedure described above. In addition, the results of on-going research suggest that the stress field modification technique can be adapted for dynamic testing to enable direct K_{IA} measurement in the future [*2a*].

Theory

Current static fracture toughness test procedures require a minimum specimen thickness to ensure plane-strain conditions are simulated in laboratory specimens. In particular, the critical fracture toughness testing parameters prescribed in ASTM E 399 [*3*] require

$$B, a_0 > 2.5 \left(\frac{K_{IC}}{\sigma_{ys}}\right)^2 \tag{1}$$

and ASTM E 813 [*4*] requires

$$B, b_0 > 25 \frac{J_{IC}}{\sigma_y} \tag{2}$$

[3] Regulatory Guide 1.99 Revision 2, "Radiation, Embrittlement of Reactor Vessel Materials," May 1988.

where

B = specimen thickness,
b_0 = uncracked ligament length,
a_0 = initial crack length,
σ_{ys} = 0.2% offset yield strength, and
σ_y = effective yield strength.

References *3* and *4* semi-empirical relationships were determined by ASTM committees using experimental data. The *J*-integral procedure enables testing with samples thinner than ASTM E 399 specimens by about a factor of 20. Reference *5* has clearly demonstrated that testing using the *J*-integral procedure yields data identical to that obtained using the Ref *3* procedures over the temperature range of validity for that procedure.

This paper reports on a new concept for fracture toughness testing. As shown schematically in Fig. 1, the new test is applicable in the region indicated, where plane stress data would be obtained using conventional methods. The basic idea is to modify the stress field in the vicinity of the crack tip to produce plane-strain conditions. The stress field modification approach uses material that is integrally machined or may be welded on the specimen sides to produce the needed through thickness material constraint to achieve plane strain conditions. This approach enables testing of very thin specimens. At present, the lower limit on thickness has not been determined. However, the early benchmark experiments have focused on the Charpy specimen thickness for application to surveillance capsule testing. It is likely that specimens with dimensions on the order of the plastic zone size, which is a

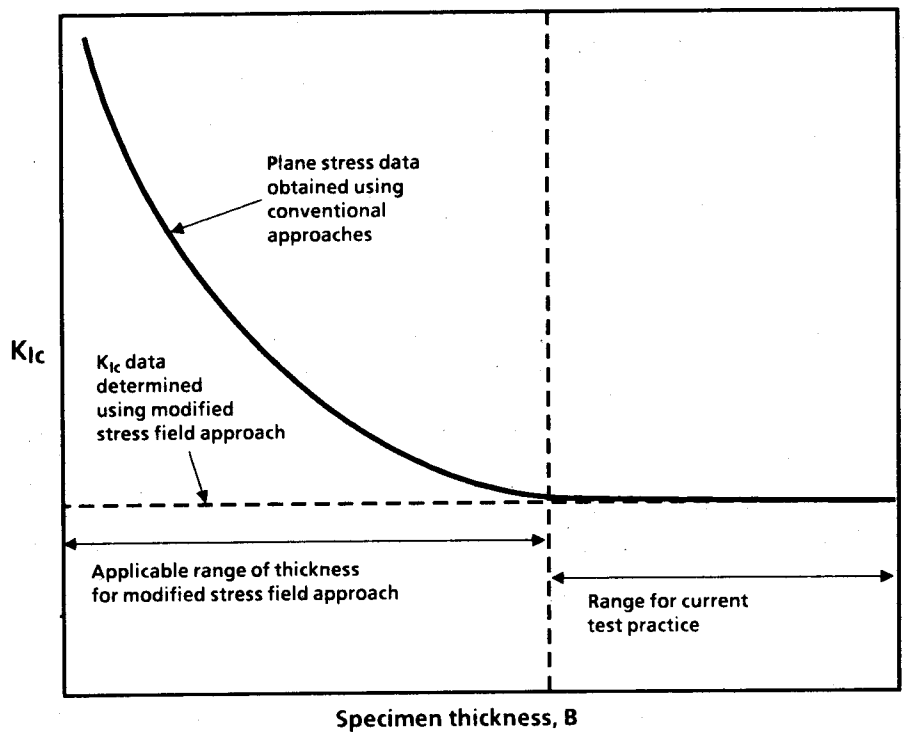

FIG. 1—*Schematic representation of the applicable range of specimen thickness* (B) *for the modified stress field approach.*

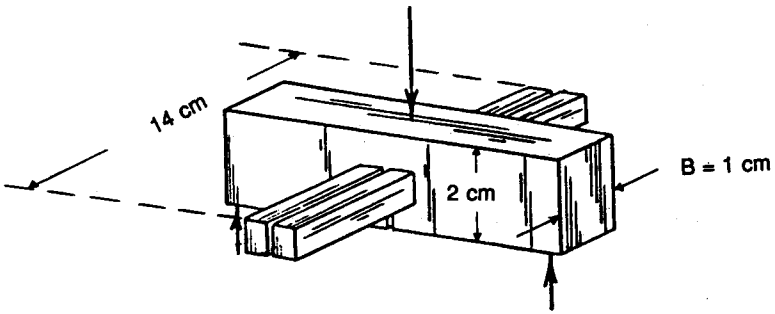

FIG. 2—*Miniaturized fracture toughness specimen design.*

function of test temperature, can be used. For pressure vessel steels, specimens with thicknesses on the order of 0.5 cm represent a practical lower bound.

There are several experimental procedures that can be used to modify the stress field. In the current study, side-constraint arms were integrally machined to simulate welded arms attached to pressure vessel surveillance specimens. Future studies will focus on solving problems associated with welding the side-constraint arms in place. The size of the arms and placement on the specimen are critical parameters in successful miniature specimen testing. Figure 2 shows the specimen design. Further details concerning specimen design are presented in Ref *6*.

In order to determine the critical experimental parameters and to validate the basic approach, two- and three-dimensional finite-element model (FEM) analyses were performed. Hence, the benchmark solution is a two-dimensional plane-strain analysis of the miniature three-point bend specimen. To validate the approach, a three-dimensional finite-element analysis of the three-point bend specimen was performed, in which the side-constraint arm was modeled so that the out-of-plane displacements on the surface are prohibited. Thus, an approximated local plane-strain condition that retains a triaxial stress state at the crack tip is achieved in the miniature specimen.

Elastic FEM Solutions

The reference formulae from the load-point displacement, the crack mouth opening, and the opening mode stress-intensity factor were reported in Ref *7* along with a comparison of the finite-element elastic solution. The key results are presented in Table 1.

The displacement solutions for the two-dimensional and the three-dimensional analyses agreed well. These solutions also agreed with the analytical load-point displacement data. The *J*-integral calculated using the two-dimensional contour integral and the virtual crack-extension (VCE) method both agreed with the analytical data to within a few percent. The approximate *J* estimated from the load versus displacement results, however, yielded data 12% higher than the analytical value. The accuracy of the approximated *J* is improved as the plastic deformation increases. These results are discussed further below.

Inelastic FEM Solutions

Reference *7* also shows the accuracy of the *J*-integral calculation in terms of its path independence for the two-dimensional analysis. Good agreement between the *J*-integral data and the virtual crack-extension data were observed.

TABLE 1—*Verification of the elastic FEM solutions at an elastic loading of P/B = 14 000 lb/in. (250 kg/cm).*

	Reference Equations	Two-Dimensional Plane Strain	% Variance from Reference Equation	Three-Dimensional With Side-Constraint	% Variation from Reference Equation
Load-Point Displacement, in. (cm)	1.770×10^{-3} (4.50×10^{-3})	1.808×10^{-3} (4.59×10^{-3})	+2.15	1.808×10^{-3} (4.59×10^{-3})	+2.15
Crack Mouth Opening Displacement, in. (cm)	1.065×10^{-3} (2.71×10^{-3})	1.053×10^{-3} (2.67×10^{-3})	−1.13	1.087×10^{-3} (2.76×10^{-3})	+2.07
J, lb/in. (kJ/m^2)	5.88 (1.03) $\left(J = \frac{K_I^2}{E'}\right)$	5.77 (1.01)	−1.87	6.623 (1.16) $\left(J = \frac{2W_i}{B(W - a)}\right)$	+12.6

Figure 3 is a plot of the load-versus-load-line displacement for the two-dimensional plane-strain analysis and the three-dimensional analysis. As anticipated, the constrained three-dimensional results are slightly softer than the two-dimensional plane-strain results, but the three-dimensional constrained data are very close to the plane-strain conditions. This result indicates that approximate plane-strain conditions were achieved using the side-constraint technique. On the other hand, the unconstrained three-dimensional results are about 12% lower in load, showing this case is rather close to the two-dimensional plane-stress conditions.

The three-dimensional finite-element data are compared with the contour J and VCE J for the two-dimensional analyses in Figs. 4 and 5. The results in these two figures show that the approximate formula for J for the constrained three-dimensional model agrees well with the rigorous plane-strain J data. Both of these curves agree well with the side-constraint data.

In addition to verifying the side constraint theory using the integral parameters discussed above, the crack tip region stress contour data were also evaluated. A comparison of the stress contour data for the case with side constraint and without indicates that the zone of

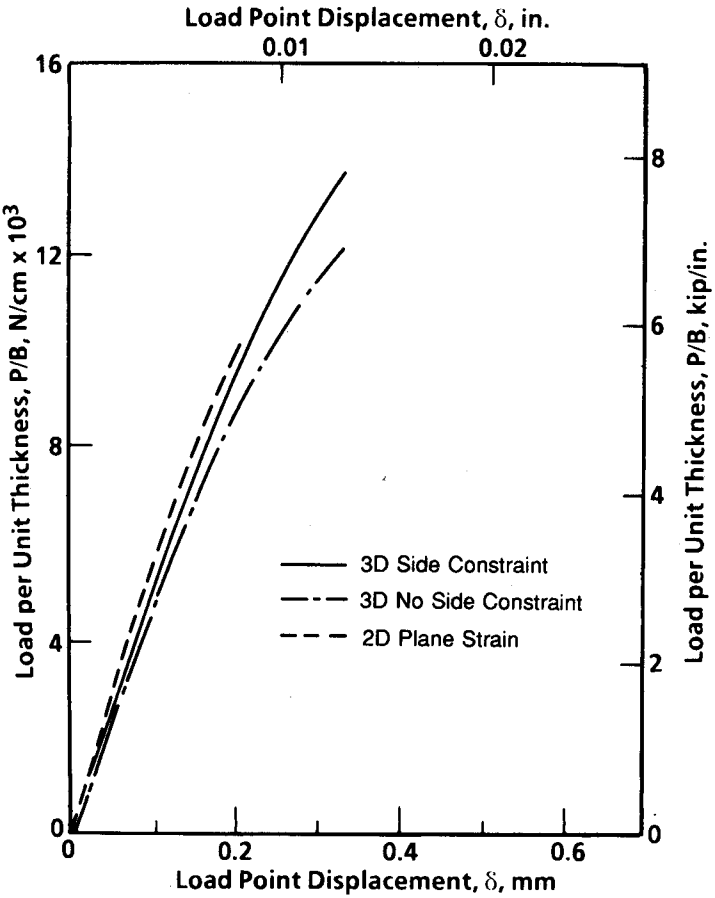

FIG. 3—*Load per unit thickness versus load-point displacement for two- and three-dimensional finite-element analyses.*

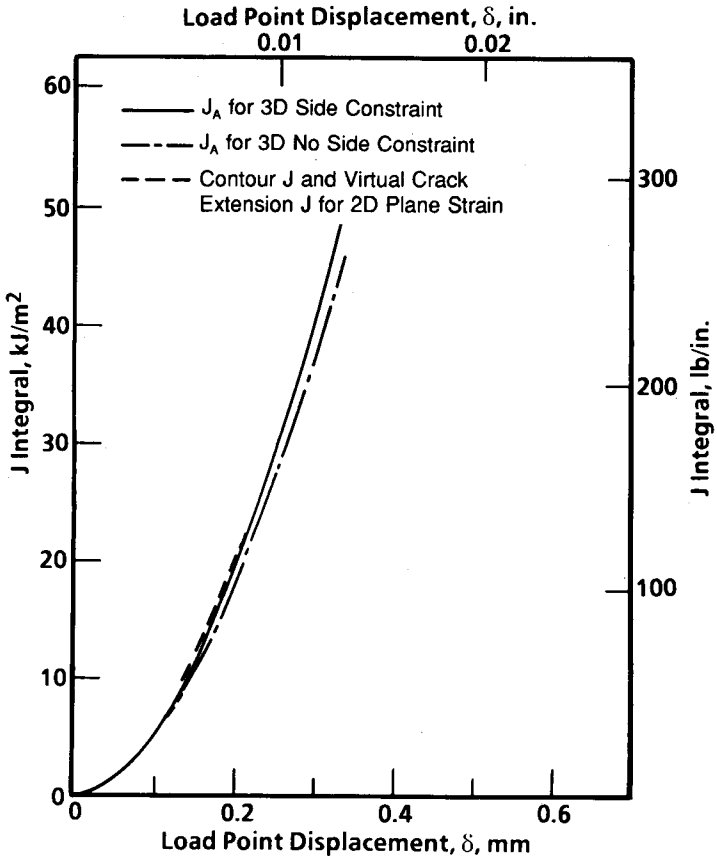

FIG. 4—*J-integral versus load-point displacement for two- and three-dimensional finite-element analyses.*

intense plastic flow in the vicinity of the crack tip is smaller for the side-constraint case. This result is expected since material constraint enhances triaxiality and thus prevents yielding by increasing the hydrostatic stress. This will reduce the plastic zone size [*8*].

Miniaturized Fracture Toughness Experiment

The test results are provided in Table 2 and Fig. 6. The specimens labeled "SC-#" are the side constraint arm tests, and these data are shown in Fig. 6. The specimens labeled "NA-#" are the "no arm" conventional specimen tests, and these data have not been included in Fig. 6 to avoid confusion. The "NA-#" tests fell within the uncertainty bands for the ORNL 0.4T data shown in Fig. 6. As indicated in Table 2, all calculations were performed in accordance with ASTM procedures. Whether ASTM E 813 or ASTM E 399 calculative methodologies were followed, the width of the crack plane (1.02 cm) was used as the specimen thickness in the mechanics equations. All other parameters have their usual definition. The electric potential method was used to detect crack initiation. The probes were attached to the specimen surface on opposite sides of the notch and spaced approximately 0.2 cm from the edge of the notch. Initiation was determined by intersecting the

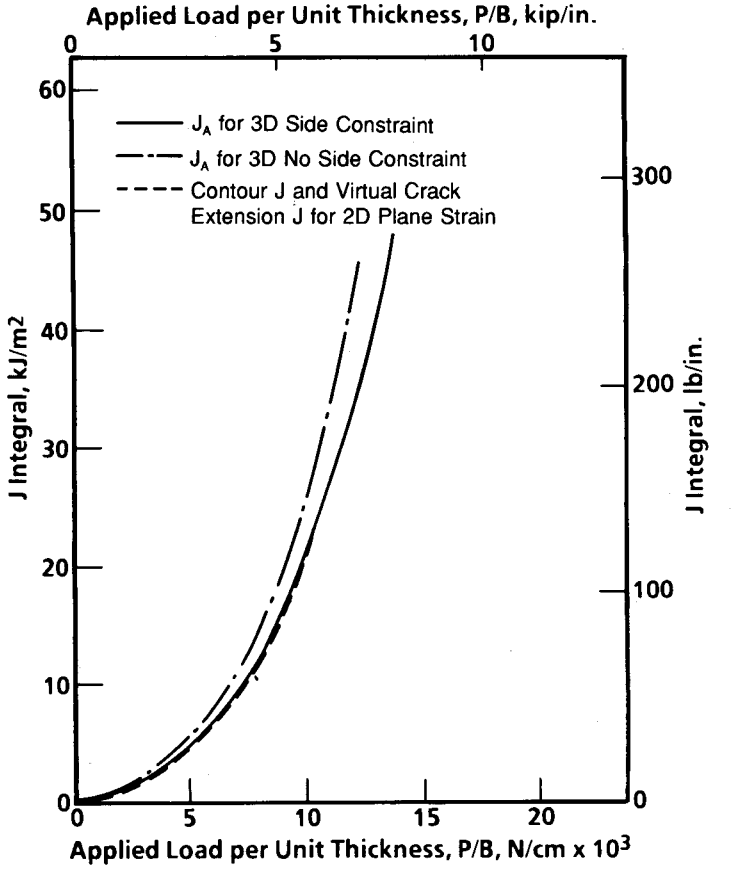

FIG. 5—*J-integral versus applied load per unit thickness for two- and three-dimensional finite-element analyses.*

baseline voltage versus loadline displacement slope with the linear slope associated with crack propagation.

Specimen NA-1 was run first at 80°C. Since ductile tearing was observed, we were concerned that this may be the fracture mode in the thick section material at that temperature. Therefore, a decision was made to run the next tests at 27°C. Specimens NA-2 and SC-3 were run next. Specimen SC-3 came close to satisfying all of the ASTM E 399 requirements. However, when Specimen NA-4 was run and it was discovered that cleavage occurred in this specimen after a very small amount of stable crack growth, we decided that a more conclusive demonstration of the success of the modified stress field approach would be obtained at 55°C. This test temperature was chosen because the specimens of the same thickness without stress field modification clearly yield K_{IC} data which are above the upper scatter band of the full thickness vessel.

Specimen NA-3 was tested at 55°C and exhibited cleavage after a large amount of ductile tearing. Specimen SC-1 was also tested at 55°C and cleavage occurred after a very small amount (0.76 mm) of stable crack growth. This specimen satisfied all of the ASTM E 399 requirements and yielded a K_{IC} value well within the scatter band of the thick section (6T vessel) data. The load versus load-point displacement data from Specimens NA-3 and SC-

TABLE 2—*Modified stress field fracture toughness data summary.*

Specimen ID	Test Temperature, °C (°F)	J_{Ic},[a] kJ/m² (in.-lb/in.²)	K_{Jc},[a] MPa$\sqrt{m}$ (ksi$\sqrt{in.}$)	K_{Ic},[b] MPa$\sqrt{m}$ (ksi$\sqrt{in.}$)	Thickness Requirement B, mm (in.)		ASTM Validity Requirements Satisfied		Fracture Mode	Ductile Crack Length, mm (in.)
					E 813	E 399	E 813	E 399		
NA-2	27 (80)	176.1 (1006)	190 (172.9)	...	5.8 (0.23)	n/a	yes	no	Ductile, terminated by cleavage	~1.6 (~0.064)
NA-4	27 (80)	126.0 (720)	161 (146.5)	...	4.3 (0.17)	...	yes	no	Cleavage after very short ductile crack	~0.5 (~0.02)
SC-3	27 (80)	162.8 (930)	183 (166.6)	88 (80.1)	5.3 (0.21)	40.6 (1.6)	yes	no[c]	Cleavage after short ductile crack	~0.5 (~0.02)
NA-3	55 (130)	266.5 (1523)	235 (213.9)	...	9.1 (0.36)	n/a	yes	no	Ductile terminated by cleavage	~6.4 (~0.25)
NA-5	55 (130)	205.3 (1173)	206 (187.5)	...	7.1 (0.28)	n/a	yes	no	Ductile	Entire ligament
SC-1	55 (130)	n/a	n/a	91 (82.8)	n/a	45.7 (1.8)	n/a	yes	Cleavage after very short ductile crack	~0.8 (~0.03)
SC-2	55 (130)	n/a	n/a	79	n/a	33.02 (1.3)	n/a	no	Cleavage after very short ductile crack	~0.8 (~0.03)
NA-1	80 (175)	249.4 (1425)	226 (205.7)	...	8.9 (0.35)	...	yes	no	Ductile	Entire ligament

[a] Determined in accordance with ASTM E 813 with initiation detected using electric potential.

[b] Determined in accordance with ASTM E 399.

[c] As a result of slippage of the COD gage, the P_{max}/P_Q requirement could not be accurately checked. The equivalent specimen thickness is 0.9 in., which does not satisfy the E 399.

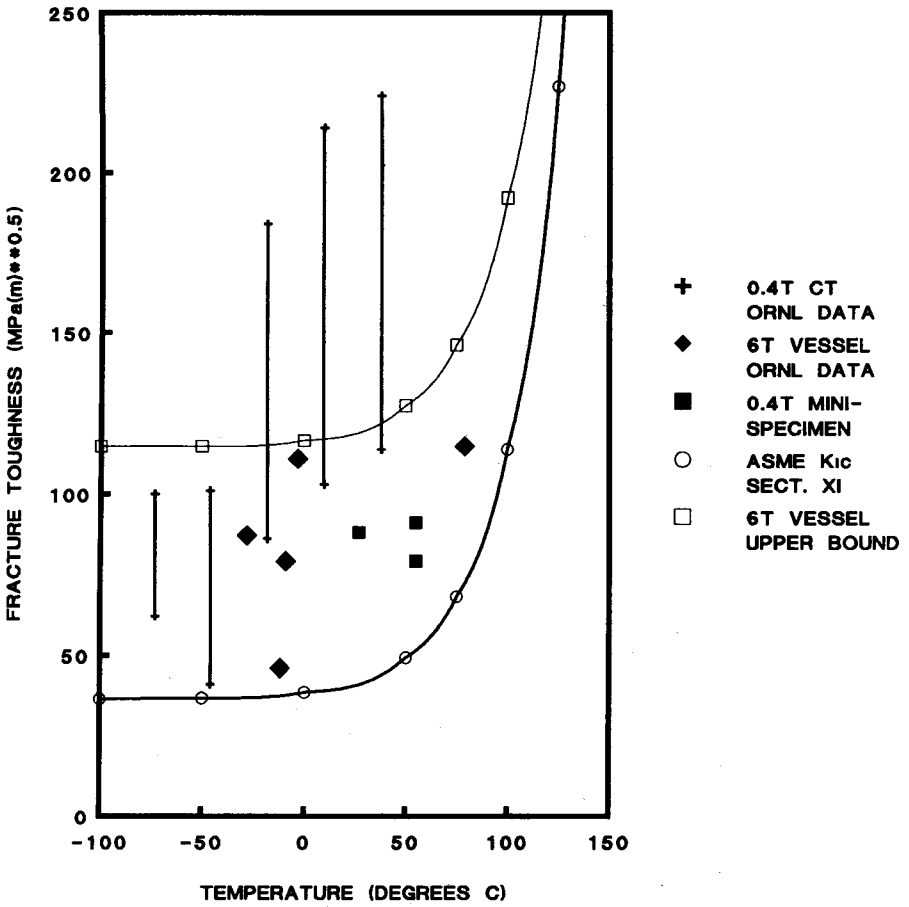

FIG. 6—*Modified stress field data compared with ORNL thick-section test results for TSE-5 and TSE-6 material.*

1 are given in Figs. 7 and 8, respectively. These data demonstrate the efficacy of the stress field modification in producing plane-strain conditions in thin specimens. Reproducibility experiments were conducted at 55°C, as shown in Fig. 6, and Specimen NA-5 yielded a high K_{JC} value and the fracture mode was entirely ductile. Specimen SC-2, like SC-1, exhibited cleavage shortly after peak load. Although this specimen did not satisfy the ASTM E 399 P_{max}/P_Q requirement, the fracture toughness data are consistent with the 6T vessel behavior.

The fracture surfaces of all the specimens tested were examined to verify the mode of fracture. Figure 9 shows the fracture surface for Specimen NA-3. Notice the large amount of stable crack growth which is terminated by cleavage. The fracture surface for the stress field-modified Specimen SC-2, tested at the same temperatures as NA-3, is given in Fig. 10. In this specimen, the fracture surface is almost entirely cleavage fracture, the exception being an initial 0.8 mm of stable crack growth. Thus, Figs. 6 through 10, the data presented in Table 2, and the results from the finite-element analysis, show that the stress field modification approach can yield data comparable to that obtained for thick section behavior (6T vessel). As shown in Fig. 6, the minaturized fracture toughness specimen data are within

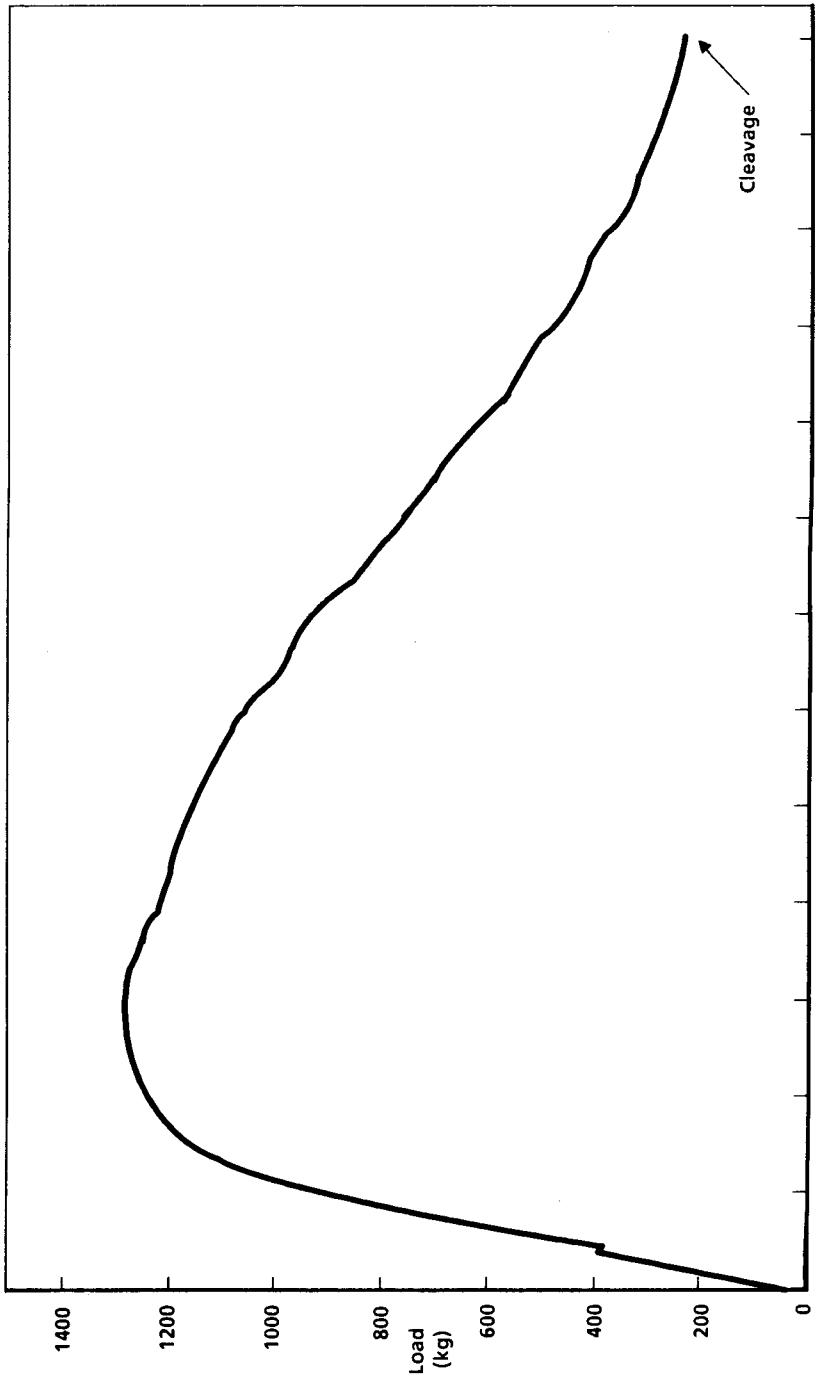

FIG. 7—*Load versus load-point displacement for Specimen NA-3.*

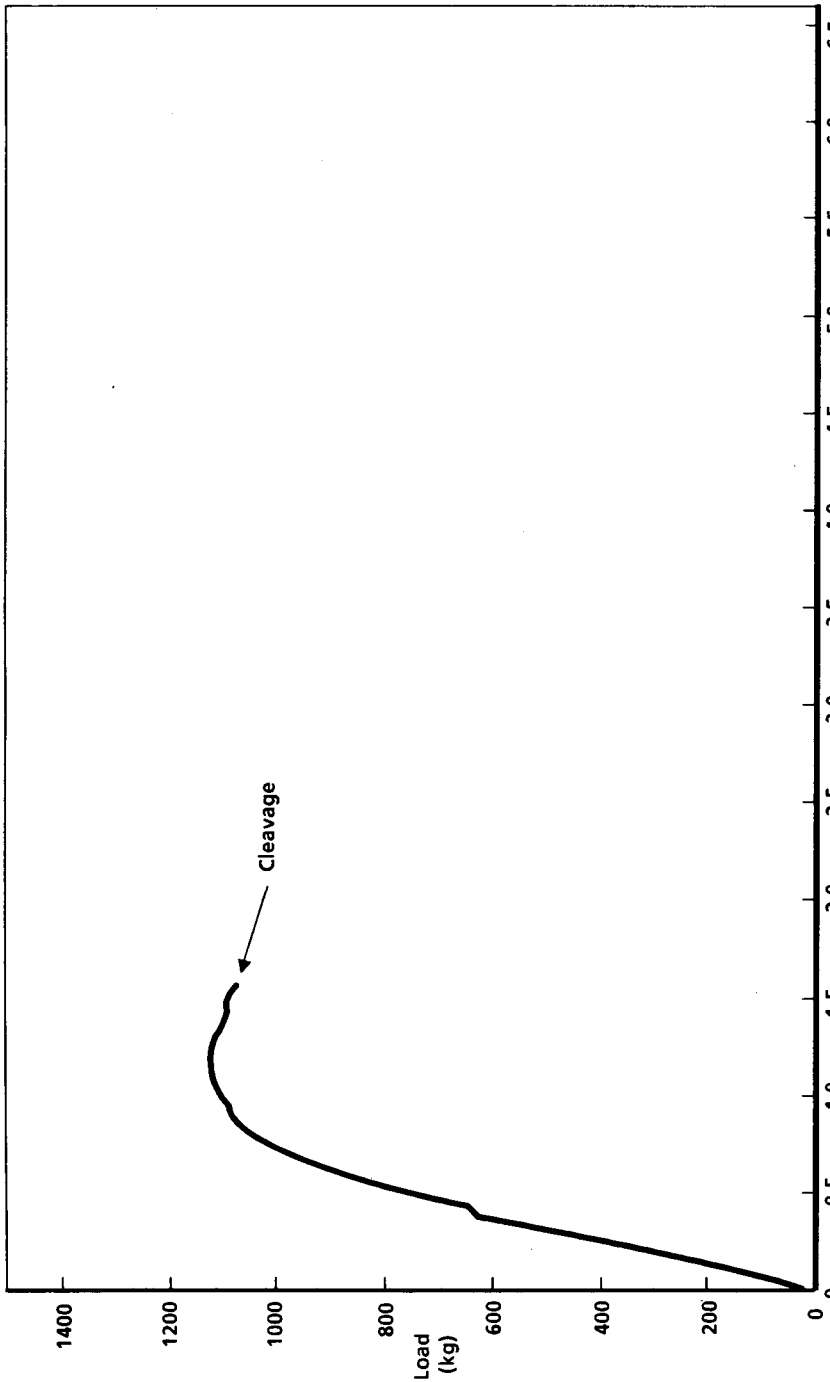

FIG. 8—*Load versus load-point displacement for Specimen SC-1.*

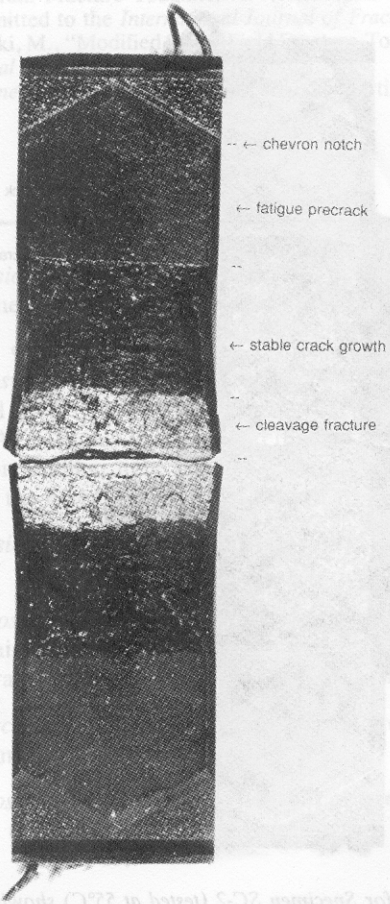

FIG. 9—*Fracture surface for Specimens NA-3 (tested at 55°C) showing predominant ductile fracture (specimen thickness = 1 cm).*

the experimental scatter of the 6T vessel data. Additional testing in the future is needed to fully characterize the uncertainty associated with miniature specimen fracture toughness testing.

Summary and Conclusions

The validity of the modified stress field theory in producing plane strain conditions in very thin specimens has been experimentally and analytically demonstrated for an ASTM A508 pressure vessel steel. The basic concept is that the small zone of intense stress in the vicinity of the crack tip controls initiation. Specimen design can achieve a modification of this field to yield plane-strain behavior in specimens which would otherwise fracture in plane stress. This approach enables testing specimens which are much thinner than those allowed by current test practices.

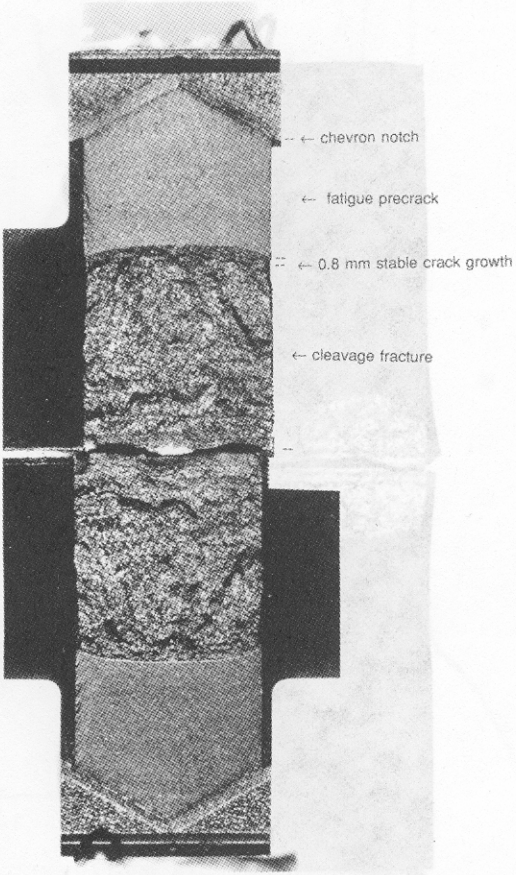

FIG. 10—*Fracture surface for Specimen SC-2 (tested at 55°C) showing predominant brittle fracture (specimen thickness = 1 cm).*

References

[*1*] Manahan, M. P., "A Comparison of Fracture Toughness Data on a Pressure Vessel with the ASME K_{IR} Curve," *Proceedings,* Seventh ASTM-EURATOM Symposium on Reactor Dosimetry, Strasbourg, France, August 1990, to be published in the conference proceedings.

[*2*] Welding Research Council, Bulletin 175, "PVRC Recommendations on Toughness Requirements for Ferritic Materials," WRC, August 1972.

[*2a*] Manahan, M. P., "Miniaturized Dynamic Fracture Toughness Measurement," patent application in preparation, 1992.

[*3*] ASTM Standard E 399, Plane-Strain Fracture Toughness of Metallic Materials, American Society for Testing and Materials, Philadelphia, PA.

[*4*] ASTM Standard E 813, Test Method for J_{IC}, A Measure of Fracture Toughness, American Society for Testing and Materials, Philadelphia, PA.

[*5*] Logsdon, W. A., "Elastic-Plastic (J_{IC}) Fracture Toughness Values: Their Experimental Determination and Comparison with Conventional Linear Elastic (K_{IC}) Fracture Toughness Values for Five Materials," *Mechanics of Crack Growth, STP 590,* American Society for Testing and Materials, Philadelphia, 1976, pp. 43–60.

[6] Manahan, M. P., "Plane-Strain Fracture Toughness Determination Using Stress Field Modified Miniature Specimens," submitted to the *International Journal of Fracture,* 1991.
[7] Manahan, M. P. and Nakagaki, M., "Modified Stress-Field Fracture-Toughness Theory Validation," submitted to the *International Journal of Fracture,* 1991.
[8] Broek, D., *Elementary Engineering Fracture Mechanics*, 4th ed., Martinus Nyhoff Publishers, 1986.

DISCUSSION

T. Sinclair[1] (*written discussion*)—How can you be certain that the welding operation does not lead to a change in toughness value on the specimen surface or lead to an uneven residual stress field in the specimen?

M. Manahan (*author's closure*)—A welding technique should be chosen which does not produce a large heat-affected zone. The laser welding approach has been chosen for further development because the HAZ is highly localized and there are several process parameters which can be adjusted. After welding, light microscopy and microhardness measurements can be made to characterize the extent of the HAZ.

R. Odette[2] (*written discussion*)—Explain how this specimen is different than very deep sidegrooves.

M. Manahan (*author's closure*)—Sidegrooves have been used in the past to constrain fracture to a plane and to straighten the crack front. Sidegrooves are not sufficient to achieve plane strain. The side constraint arms reported in my paper yield plane-strain conditions.

F. M. Haggag[3] (*written discussion*)—What is (if any) the requirement for material choice for use as constraint side arms in your test?

M. Manahan (*author's closure*)—The side constraint arm material must be compatible, in terms of weldability, with the material being tested.

[1] Mechanical Engineering Dept., University of Toronto, Canada.
[2] University of California at Santa Barbara.
[3] Oak Ridge National Laboratory, Oak Ridge, TN.